Supporting Information
for

Enhanced Oxygen Ion Conductivity and Mechanistic Understanding in $Ba_3Nb_{1-x}V_xMoO_{8.5}$

Sacha Fop,*,† Kirstie McCombie, † Ronald I. Smith‡ and Abbie C. Mclaughlin *,†

† Department of Chemistry, University of Aberdeen, Meston Walk, Aberdeen AB24 3UE, United Kingdom.

‡ ISIS Facility, Rutherford Appleton Laboratory, Harwell, Didcot OX11 0DE, United Kingdom.

* sacha.fop1@abdn.ac.uk

* a.c.mclaughlin@abdn.ac.uk

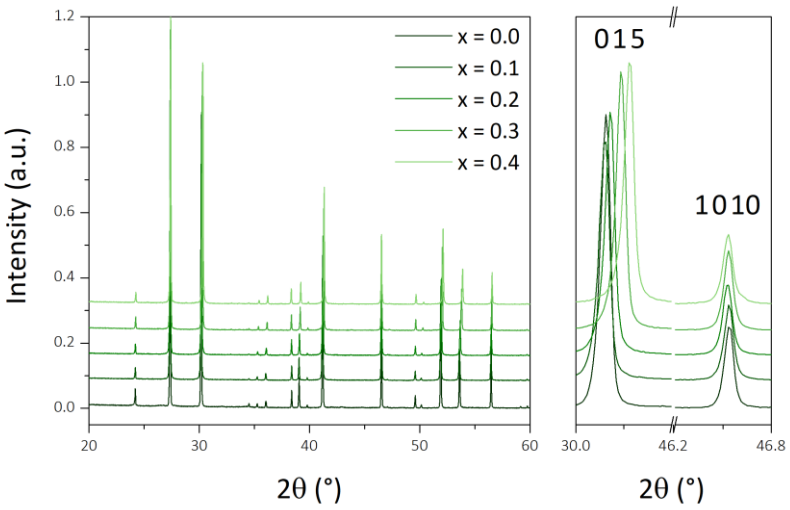

Supporting Figure S1. Laboratory X-ray diffraction patterns of the $Ba_3Nb_{1-x}V_xMoO_{8.5}$ (*x* = 0.0, 0.1, 0.2, 0.3, 0.4) series. The right panel shows the anisotropic shift of selected reflections.

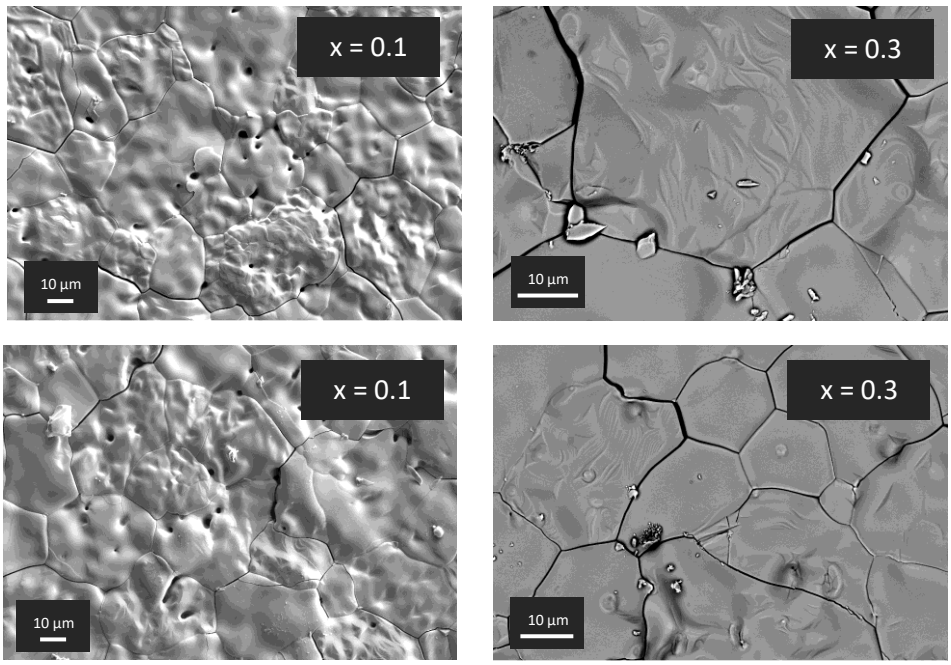

Supporting Figure S2. SEM micrographs of the surface of as prepared pellets of selected members of the $Ba_3Nb_{1-x}V_xMoO_{8.5}$ series. Secondary electron (SE) and backscattering (BSE) images are shown on the left and on the right respectively.

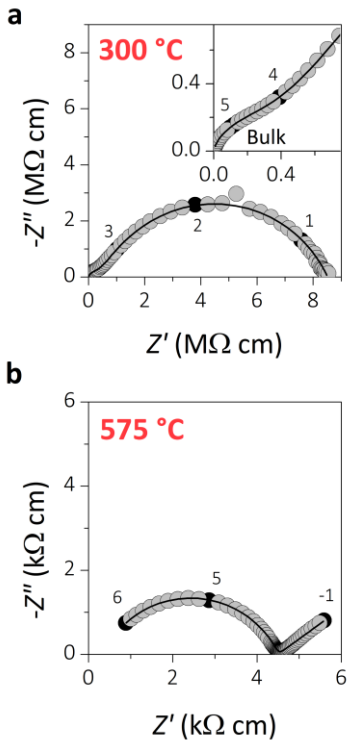

Supporting Figure S3. Complex impedance plots of the parent $Ba_3Nb_{1-x}V_xMoO_{8.5}$ x = 0.0 composition recorded at 300 °C (a) and 575 °C (b). Inset in (a) shows a magnification of the high frequency region. The numbers and corresponding filled circles indicate selected frequency decades; the black line is the equivalent circuit fitting.

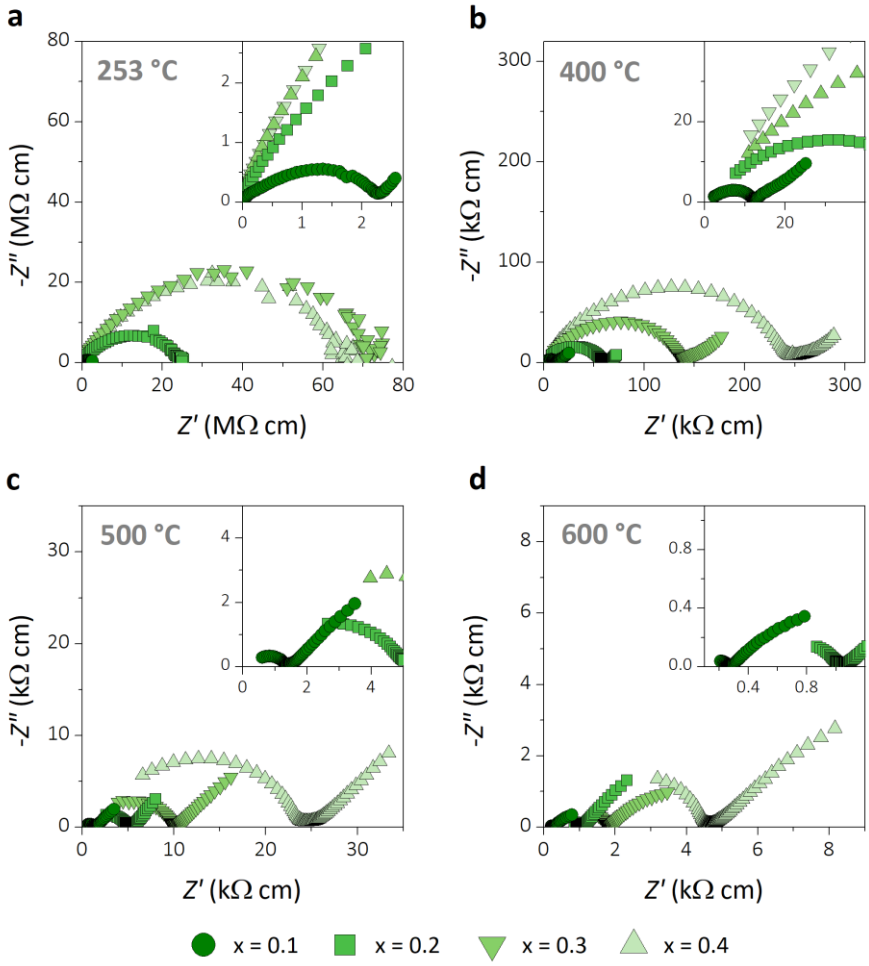

Supporting Figure S4. Complex impedance plots of the doped $Ba_3Nb_{1-x}V_xMoO_{8.5}$ (x = 0.1, 0.2, 0.3, 0.4) compositions recorded at 253 °C (a), 400 °C (b), 500 °C (c) and 600 °C (d). The insets show magnification of the $Ba_3Nb_{0.9}V_{0.1}MoO_{8.5}$ data.

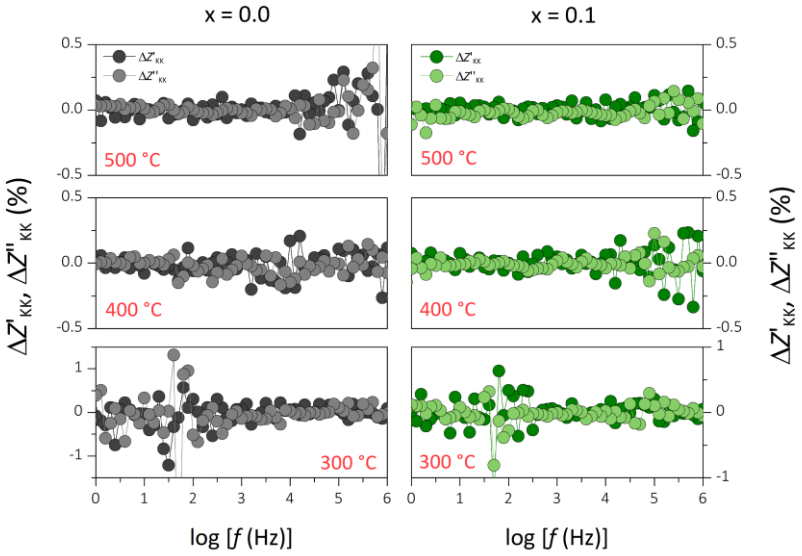

Supporting Figure S5. Typical residual plots for the samples with *x* = 0.0 and 0.1 obtained from the Kramers-Kronig (KK) tests at selected temperatures. Kramers-Kronig validation ensures that the impedance response is a representation of a linear, time-invariant (i.e. the measured cell is in equilibrium) and casual system. KK relations relate the real and imaginary parts of the impedance spectrum to each other, and properly collected impedance data must obey these KK relations [1]. The random distribution of the residuals around the frequency axis indicate that the system complies with the KK relations and therefore the effectiveness of the collected data [2].

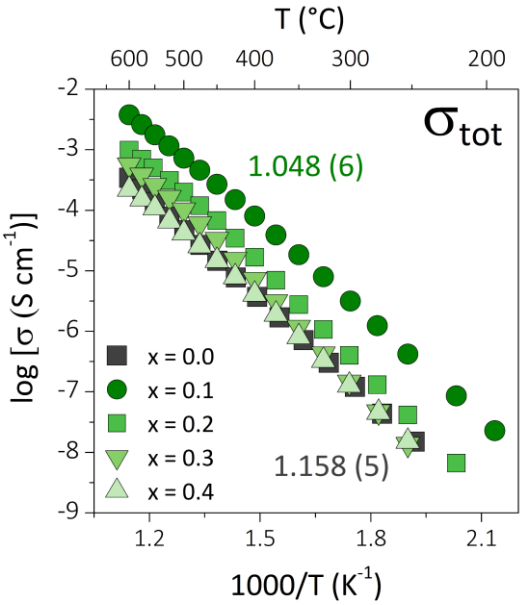

Supporting Figure S6. Arrhenius plot of the total ionic conductivity of $Ba_3Nb_{1-x}V_xMoO_{8.5}$ (x = 0.0, 0.1, 0.2, 0.3, 0.4). Activation energy values (in eV) are reported for x = 0.0 and 0.1.

Equivalent circuit analysis

An equivalent circuit (EC) fitting procedure was employed to extract the individual bulk, grain boundary and electrode responses for the impedance data of the $Ba_3Nb_{1-x}V_xMoO_{8.5}$ series. The equivalent circuits depicted in Supporting Figure S7 were used to model the impedance data.

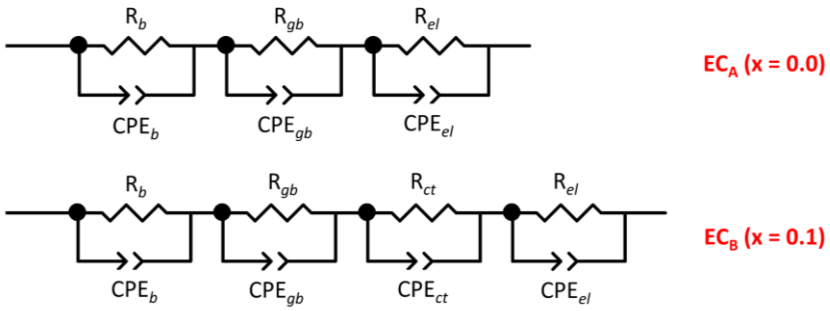

Supporting Figure S7. Equivalent circuits used to model the impedance data of the parent compound (EC_A) and of $Ba_3Nb_{0.9}V_{0.1}MoO_{8.5}$ (EC_B). R indicates a resistor, while CPE is a constant phase element; the subscript *b* stands for bulk, *gb* for grain boundary, *el* for electrode and *ct* for charge transfer.

The equivalent circuit EC_A was employed to model the data of the sample with composition $x = 0.0$, in agreement with a previous report on $Ba_3NbMoO_{8.5}$ [3]. At the lower temperatures, the complex impedance data show the high-frequency bulk signal and the grain boundary arc at intermediate-low frequencies. The electrode response at low frequencies is clearly visible only for T ≥ 375 °C; the parallel $(R\text{-}CPE)_{el}$ element was utilized from that temperature. Above 450 °C, the bulk signal moves outside the frequency range of the scan; the $(R\text{-}CPE)_b$ element for the bulk response is substituted by a series resistance, R_b, followed by the (R-CPE) elements for the grain boundary and electrode responses. The equivalent circuit EC_B was used for the impedance data of $Ba_3Nb_{0.9}V_{0.1}MoO_{8.5}$. The complex impedance data is composed by poorly resolved bulk and grain boundary arcs, together with a pronounced Warburg signal in the low frequency region. At 400 °C, a charge transfer feature associated with charge transfer to and from the oxide ions at the electrode-ceramic interface appears between the grain arc and the electrode signal and is modelled with a $(R\text{-}CPE)_{ct}$ element [4]. The charge transfer

feature becomes less prominent as the temperature rises. For T ≥ 425 °C, the $(R\text{-}CPE)_b$ element for the bulk response is substituted by a series resistance, R_b. The obtained bulk and grain boundary resistivity values and CPE parameters for x = 0.0 and 0.1 are reported in Supporting Table S1. Similar equivalent circuit modelling was employed to extract bulk and grain boundary conductivity values also for the compositions with x = 0.2, 0.3, 0.4. The bulk conductivities for all the compositions are presented in the Arrhenius plot in Supporting Figure S10.

Equivalent circuit fits for x = 0.0 and 0.1 at selected temperatures are presented in Supporting Figure S8, and in Figure 1a, b in the main manuscript. The good match between the observed and calculated spectra is evident from the graphs.

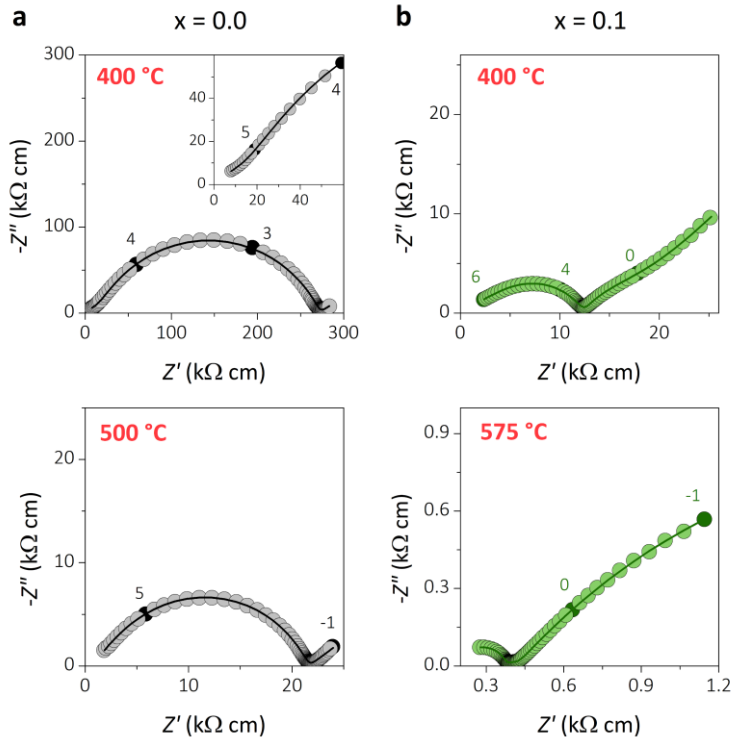

Supporting Figure S8. Representitive equivalent circuit fit of complex impedance data collected on $Ba_3Nb_{1-x}V_xMoO_{8.5}$ with x = 0.0 (a) and 0.1 (b). Inset in (a) shows a magnification of the high frequency region. The numbers and corresponding filled circles indicate selected frequency decades; lines are the equivalent circuit fitting.

The residuals from the equivalent circuit analysis ($\Delta Z'_{EC}$, $\Delta Z''_{EC}$) present small values, with a variation generally smaller than 0.02%, and are reasonably scattered along log(f) (Supporting Figure S9), further validating the quality of the employed model [2].

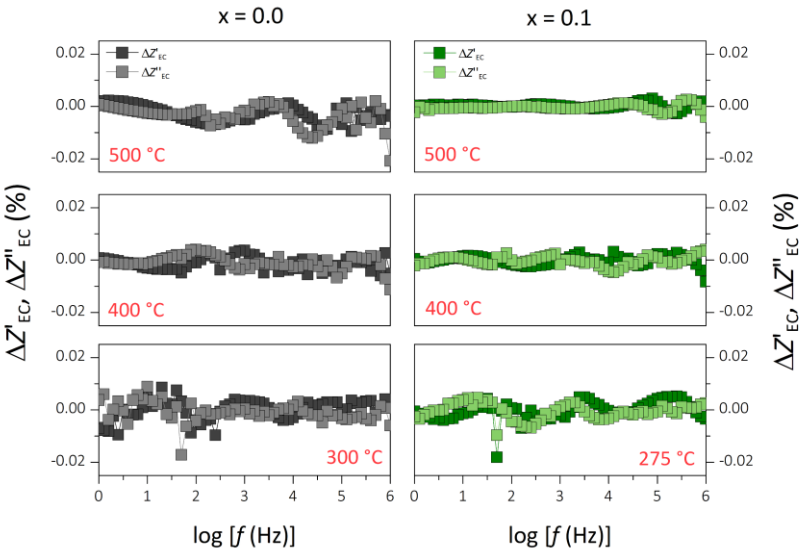

Supporting Figure S9. Typical residual plots of the equivalent circuit fitting procedure at selected temperatures. The good match between observed and calculated impedance data, and the random distribution of the residuals indicate that the employed equivalent circuit models adequately represent the collected data.

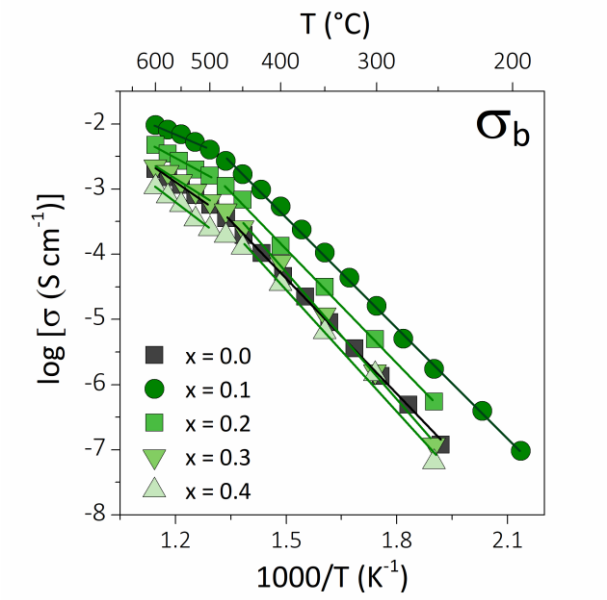

Supporting Figure S10. Arrhenius plot of the bulk ionic conductivity of $Ba_3Nb_{1-x}V_xMoO_{8.5}$ (*x* = 0.0, 0.1, 0.2, 0.3, 0.4). The lines show the linear fit to the data.

Supporting Table S1. Equivalent circuit fitting parameters obtained for the bulk and grain boundary responses of $Ba_3Nb_{1-x}V_xMoO_{8.5}$ with x = 0.0 and 0.1. The complex impedance of a constant phase element is defined as $Z_{CPE} = 1/[Q(j\omega)^n]$, where j is the imaginary unit and ω the radial frequency.

x = 0.0						
T (°C)	**R_b (Ω cm)**	**Q_b (Ω^{-1} s^{-1})**	**n_b**	**R_{gb} (Ω cm)**	**Q_{gb} (Ω^{-1} s^{-1})**	**n_{gb}**
248	8.42×10^6	5.4×10^{-11}	0.75	5.80×10^7	7.8×10^{-10}	0.75
275	2.03×10^6	5.8×10^{-11}	0.78	2.09×10^7	1.1×10^{-9}	0.74
300	7.40×10^5	6.9×10^{-11}	0.75	7.57×10^6	1.4×10^{-9}	0.71
325	2.80×10^5	8.3×10^{-11}	0.79	3.04×10^6	1.8×10^{-9}	0.71
345	1.11×10^5	9.0×10^{-11}	0.79	1.28×10^6	2.3×10^{-9}	0.73
375	4.47×10^4	1.4×10^{-10}	0.77	5.44×10^5	2.3×10^{-9}	0.73
400	2.16×10^4	2.9×10^{-10}	0.76	2.50×10^5	2.7×10^{-9}	0.74
425	9.62×10^3	3.0×10^{-10}	0.75	1.20×10^5	3.7×10^{-9}	0.75
450	5.09×10^3	5.4×10^{-10}	0.74	6.34×10^4	3.9×10^{-9}	0.73
475	2.83×10^3	-	-	3.45×10^4	5.5×10^{-9}	0.73
500	1.77×10^3	-	-	1.98×10^4	8.7×10^{-9}	0.71
525	1.23×10^3	-	-	1.16×10^4	9.4×10^{-9}	0.72
550	8.72×10^2	-	-	6.48×10^3	1.0×10^{-8}	0.72
575	6.57×10^2	-	-	3.84×10^3	1.0×10^{-8}	0.72
600	4.97×10^2	-	-	2.41×10^3	1.3×10^{-8}	0.72
x = 0.1						
T (°C)	**R_b (Ω cm)**	**Q_b (Ω^{-1} s^{-1})**	**n_b**	**R_{gb} (Ω cm)**	**Q_{gb} (Ω^{-1} s^{-1})**	**n_{gb}**
195	1.05×10^7	8.2×10^{-11}	0.75	3.35×10^7	8.1×10^{-10}	0.72
220	2.56×10^6	8.7×10^{-11}	0.77	9.12×10^6	8.9×10^{-10}	0.70
253	5.74×10^5	1.8×10^{-10}	0.75	1.79×10^6	9.6×10^{-10}	0.74
275	1.96×10^5	2.3×10^{-10}	0.75	6.12×10^5	9.9×10^{-10}	0.76
300	6.24×10^4	2.5×10^{-10}	0.77	2.55×10^5	2.0×10^{-9}	0.71
325	2.31×10^4	3.4×10^{-10}	0.76	1.03×10^5	2.1×10^{-9}	0.72
350	9.44×10^3	5.6×10^{-10}	0.75	4.50×10^4	2.5×10^{-9}	0.72
375	4.20×10^3	8.3×10^{-10}	0.74	2.14×10^4	3.0×10^{-9}	0.72
400	1.87×10^3	8.8×10^{-10}	0.75	1.06×10^4	3.6×10^{-9}	0.72
425	1.02×10^3	-	-	5.63×10^3	3.9×10^{-9}	0.73
450	5.97×10^2	-	-	3.10×10^3	4.2×10^{-9}	0.73
475	3.69×10^2	-	-	1.81×10^3	4.3×10^{-9}	0.75
500	2.46×10^2	-	-	1.11×10^3	5.5×10^{-9}	0.74
525	1.89×10^2	-	-	6.72×10^2	5.8×10^{-9}	0.74
550	1.45×10^2	-	-	4.21×10^2	6.9×10^{-9}	0.73
575	1.22×10^2	-	-	2.62×10^2	8.5×10^{-9}	0.73
600	1.03×10^2	-	-	1.62×10^2	9.5×10^{-9}	0.73

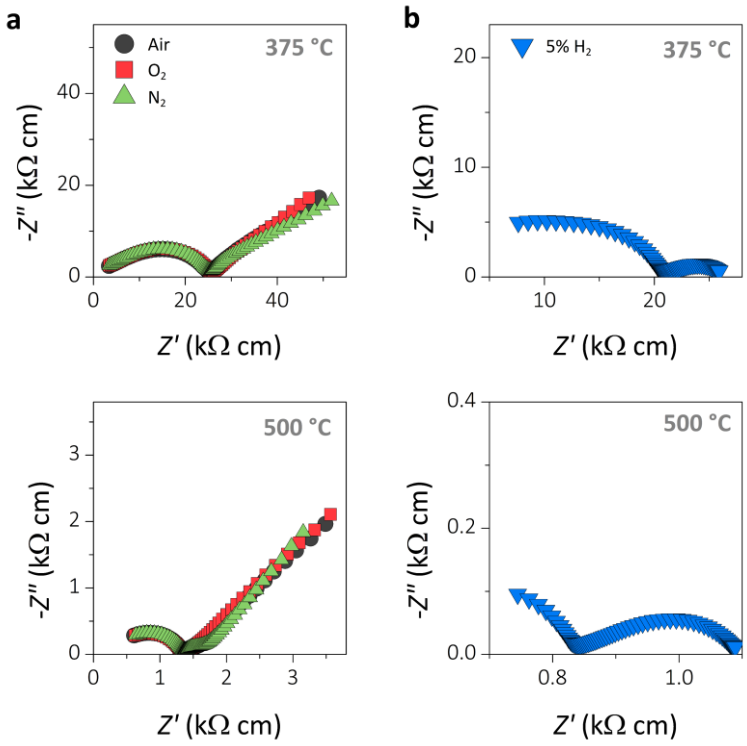

Supporting Figure S11. Complex impedance plots of $Ba_3Nb_{0.9}V_{0.1}MoO_{8.5}$ recorded under high and intermediate pO_2 conditions (a), and measured under reducing 5% H_2 (in N_2) atmosphere (b). The behavior of the grain arc and the low frequency data under high and intermediate pO_2 conditions is consistent with solid oxygen ionic conduction [5]. The slighlty reduced resistivity values in 5% H_2 (in N_2) atmosphere suggest electronic conduction, however the presence of clear Warburg/electrode responses at all temperatures indicates that the electronic component is small and the conductivity is predominantly ionic [6].

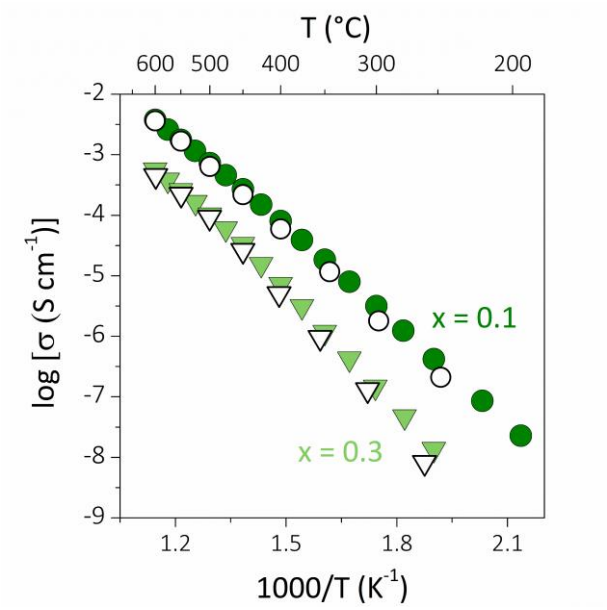

Supporting Figure S12. Arrhenius plot of the total ionic conductivity of $Ba_3Nb_{1-x}V_xMoO_{8.5}$ with x = 0.1 and 0.3 recorded in dry air ($pH_2O < 10^{-4}$ atm, filled symbols) and humidified air (pH_2O ~ 0.021 atm, empty symbols).

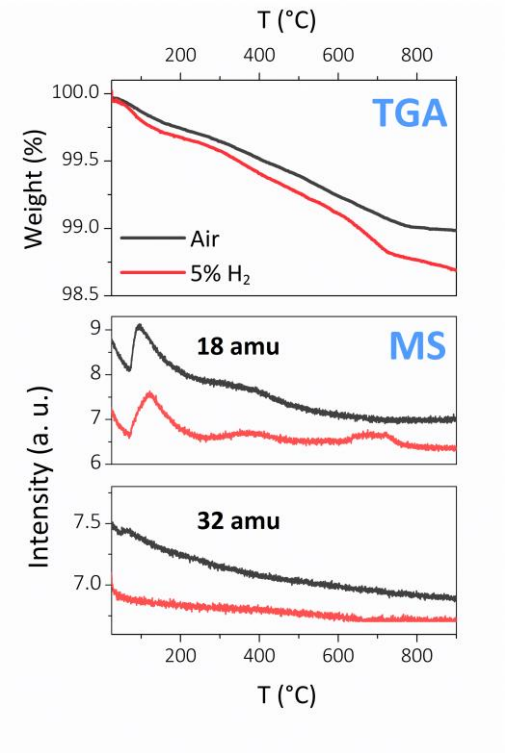

Supporting Figure S13. Results of the TGA-MS analysis on a $Ba_3Nb_{0.9}V_{0.1}MoO_{8.5}$ sample under dry air and 5% H_2 (in N_2) atmospheres. The top panel shows the thermogravimetric (TGA) diagram, while the bottom ones are the mass spectroscopy diagrams obtained at 18 amu (H_2O) and 32 amu (O_2).

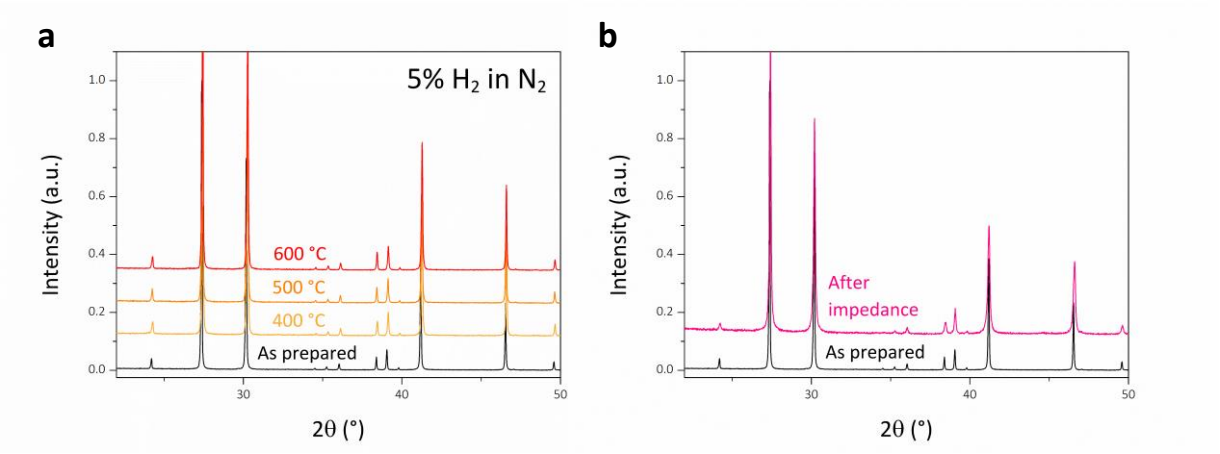

Supporting Figure S14. XRD pattern of $Ba_3Nb_{0.9}V_{0.1}MoO_{8.5}$ after annealing for 24 h at various temperatures under 5% H_2 (in N_2) (a) and after the impedance spectroscopy tests (b).

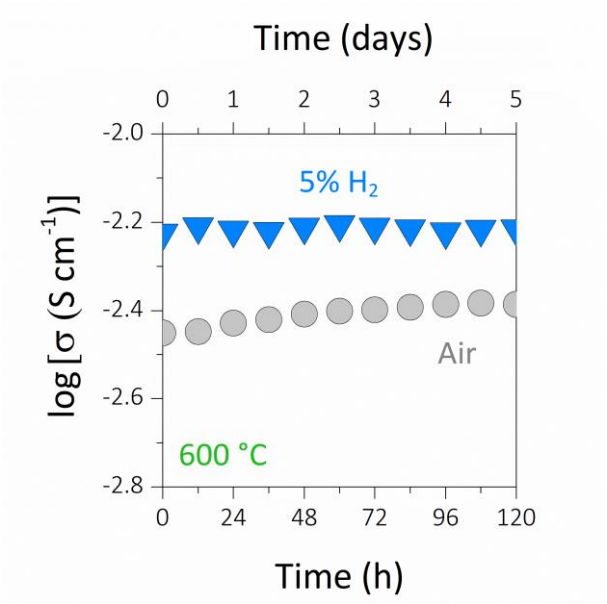

Supporting Figure S15. Variation with time of the total conductivity of $Ba_3Nb_{0.9}V_{0.1}MoO_{8.5}$ at 600 °C measured under air and 5% H_2 (in N_2).

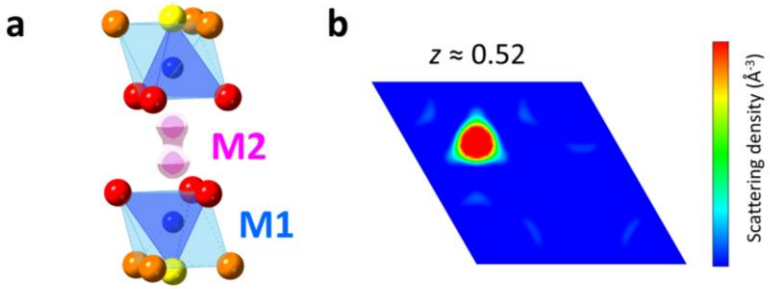

Supporting Figure S16. Volumetric data from difference Fourier analysis on $Ba_3Nb_{0.9}V_{0.1}MoO_{8.5}$ evidencing that the M2 cation is split on the (0,0, ~0.52) 6*c* position, instead of occupying the nominal 3*b* position at the centre of the octahedral cavity (a). Difference Fourier map at $z \sim 0.52$ seen along the [001] direction.

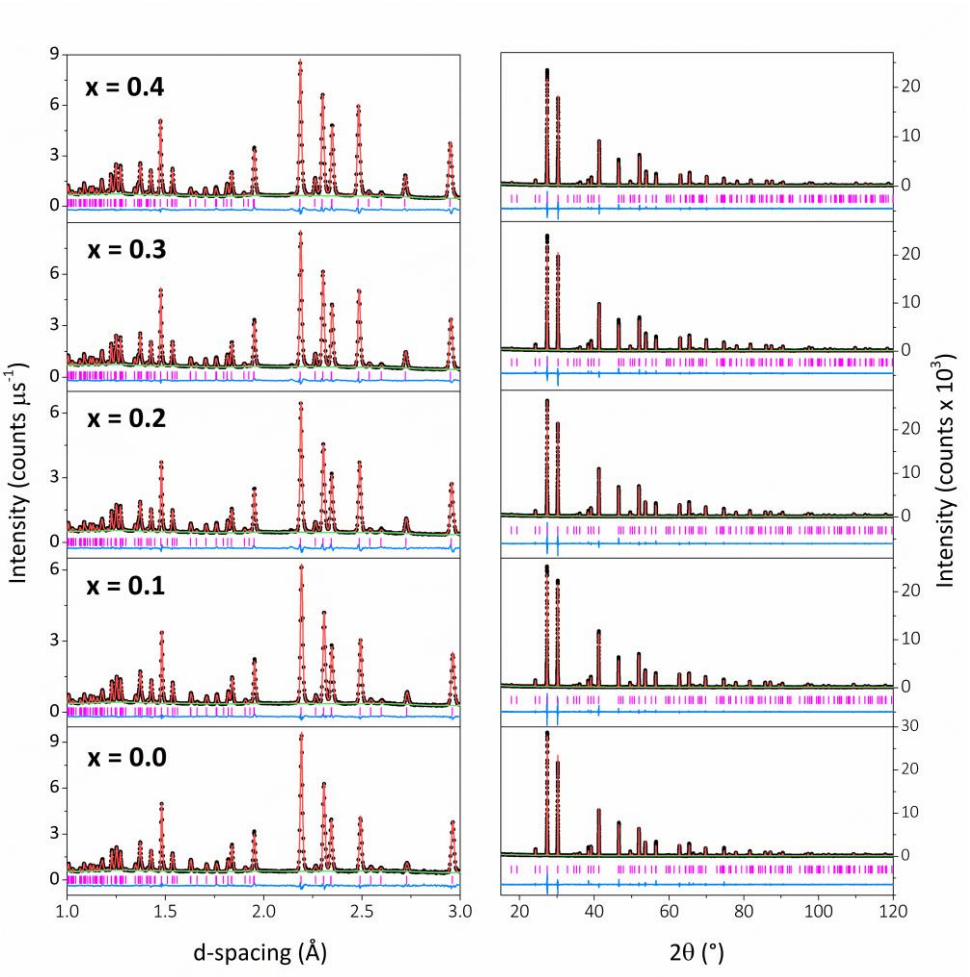

Supporting Figure S17. Rietveld fit to the structural model of $Ba_3Nb_{1-x}V_xMoO_{8.5}$ (x = 0.0, 0.1, 0.2, 0.3, 0.4) from neutron (left) and X-ray (right) diffraction data. The neutron data collected by the 90° detector bank of the POLARIS instrument is shown. Black dots indicate the observed data, the red line the Rietveld fit, the blue line the difference between the observed and calculated patterns, the green line the background function, and the pink bars the reflection positions.

Supporting Table S2. Refined atomic parameters from Rietveld fit of the powder diffraction data of $Ba_3Nb_{1-x}V_xMoO_{8.5}$ (x = 0.0, 0.1, 0.2, 0.3, 0.4). Data were refined in the space group $R\bar{3}m$ *H*. Thermal displacement parameters are reported in $Å^2$. Rwp values from refinement of the model from XRD data are reported in square brackets.

		x = 0.0	**x = 0.1**	**x = 0.2**	**x = 0.3**	**x = 0.4**
***a* (Å)**		5.91971 (6)	5.92018 (5)	5.90966 (6)	5.90179 (5)	5.89516 (5)
***c* (Å)**		21.0787 (2)	21.1009 (2)	21.1100 (3)	21.1167 (2)	21.1241 (2)
V (Å³)		639. 700 (1)	640.490 (1)	638.744 (2)	636.978 (2)	635.769 (1)
		x = 0.0	**x = 0.1**	**x = 0.2**	**x = 0.3**	**x = 0.4**
Ba1 (0,0,0) 3*a*	$U_{11} = U_{22}$	0.0202 (9)	0.0225 (6)	0.0221 (7)	0.0181 (5)	0.0202 (5)
	U_{33}	0.0062 (2)	0.0142 (1)	0.0118 (2)	0.0142 (7)	0.0134 (8)
	U_{12}	0.0101 (5)	0.0114 (3)	0.0110 (3)	0.0074 (2)	0.0101 (3)
Ba2 (0,0,*z*) 6*c*	***z***	0.2069 (1)	0.20687 (8)	0.20662 (8)	0.20670 (7)	0.20659 (6)
	$U_{11} = U_{22}$	0.0111 (5)	0.0183 (4)	0.0161 (4)	0.0156 (3)	0.0176 (3)
	U_{33}	0.0420 (1)	0.0396 (6)	0.0414 (8)	0.0389 (6)	0.0377 (6)
	U_{12}	0.0055 (2)	0.0093 (2)	0.0081 (2)	0.0062 (2)	0.0088 (2)
M1 (0,0,*z*) 6*c*	***z***	0.39851 (6)	0.39855 (5)	0.39877 (5)	0.39862 (4)	0.39874 (5)
	Frac (Nb1)	0.443 (1)	0.410 (2)	0.374 (1)	0.330 (1)	0.285 (1)
	Frac (Mo1)	0.443 (1)	0.449 (2)	0.459 (1)	0.465 (1)	0.475 (1)
	Frac (V1)	–	0.029 (2)	0.069 (1)	0.112 (1)	0.165 (1)
	$U_{11} = U_{22}$	0.0074 (3)	0.0099 (3)	0.0112 (2)	0.0103 (2)	0.0118 (2)
	U_{33}	0.0309 (9)	0.0345 (7)	0.0316 (8)	0.0268 (6)	0.0234 (6)
	U_{12}	0.0037 (2)	0.0050 (1)	0.0056 (2)	0.0052 (1)	0.0059 (1)
M2 (0,0,*z*) 6*c*	***z***	0.5220 (2)	0.5240 (3)	0.5257 (4)	0.5270 (4)	0.5291 (6)
	Frac (Nb2)	0.057 (1)	0.040 (2)	0.026 (1)	0.020 (1)	0.015 (1)
	Frac (Mo2)	0.057 (1)	0.051 (2)	0.041 (1)	0.035 (1)	0.025 (1)
	Frac (V2)	–	0.020 (2)	0.031 (1)	0.038 (1)	0.035 (1)
	U_{iso}	0.0095 (2)	0.0077 (5)	0.0085 (3)	0.0099 (2)	0.008 (1)
O1 ($x,\bar{x},z$) 18*h*	***x***	0.17275 (7)	0.17234 (5)	0.17232 (6)	0.17239 (4)	0.17235 (5)
	y	0.82724 (7)	0.82765 (5)	0.82766 (6)	0.82759 (4)	0.82764 (5)
	z	0.10392 (3)	0.10332 (2)	0.10284 (2)	0.10263 (2)	0.10226 (2)
	$U_{11} = U_{22}$	0.0237 (3)	0.0261 (2)	0.0256 (3)	0.0236 (2)	0.0241 (2)
	U_{33}	0.0191 (4)	0.0212 (3)	0.0195 (4)	0.0185 (3)	0.0178 (3)
	U_{12}	0.0185 (3)	0.0194 (3)	0.0196 (3)	0.0183 (2)	0.0189 (2)
	U_{13}	0.009 (1)	0.0013 (1)	0.006 (1)	0.008 (1)	0.009 (1)
	U_{23}	-0.009 (1)	-0.0013 (1)	-0.006 (1)	-0.008 (1)	-0.009 (1)

Supporting Table S2. Continued.

		x = 0.0	x = 0.1	x = 0.2	x = 0.3	x = 0.4
O2 (0.5,0,0) 9*e*	**Frac**	0.467 (2)	0.435 (2)	0.405 (1)	0.396 (2)	0.376 (2)
	U_{11}	0.0192 (6)	0.0217 (6)	0.0226 (8)	0.0267 (7)	0.0285 (7)
	U_{22}	0.054 (1)	0.047 (1)	0.051 (1)	0.049 (1)	0.052 (1)
	U_{33}	0.0330 (6)	0.0321 (4)	0.0354 (7)	0.0320 (6)	0.033 (1)
	U_{12}	0.0273 (8)	0.0238 (5)	0.0255 (7)	0.0247 (6)	0.0260 (6)
	U_{13}	0.0197 (7)	0.0171 (5)	0.0198 (7)	0.0185 (5)	0.0189 (6)
	U_{23}	0.0933 (1)	0.0343 (6)	0.039 (1)	0.037 (1)	0.037 (1)
O3 (*x,y,z*) 36*i*	***x***	0.0939 (6)	0.0873 (5)	0.0839 (6)	0.0794 (4)	0.0742 (4)
	y	0.0852 (7)	0.0792 (7)	0.0676 (8)	0.0627 (8)	0.0594 (8)
	z	0.3216 (2)	0.3221 (1)	0.3231 (1)	0.3236 (1)	0.32393 (9)
	Frac	0.092 (1)	0.100 (2)	0.107 (1)	0.109 (2)	0.114 (2)
	U_{iso}	0.031 (1)	0.037 (1)	0.037 (1)	0.0360 (8)	0.0314 (7)
		x = 0.0	**x = 0.1**	**x = 0.2**	**x = 0.3**	**x = 0.4**
χ^2		1.99	2.23	2.97	3.85	3.51
Rp (%)		3.20	3.31	3.30	2.38	2.44
Rwp (%)		2.41 [5.36]	1.93 [5.21]	1.99 [6.12]	1.77 [5.79]	1.68 [5.31]
RF2 (%)		2.79	2.06	1.71	1.70	1.80

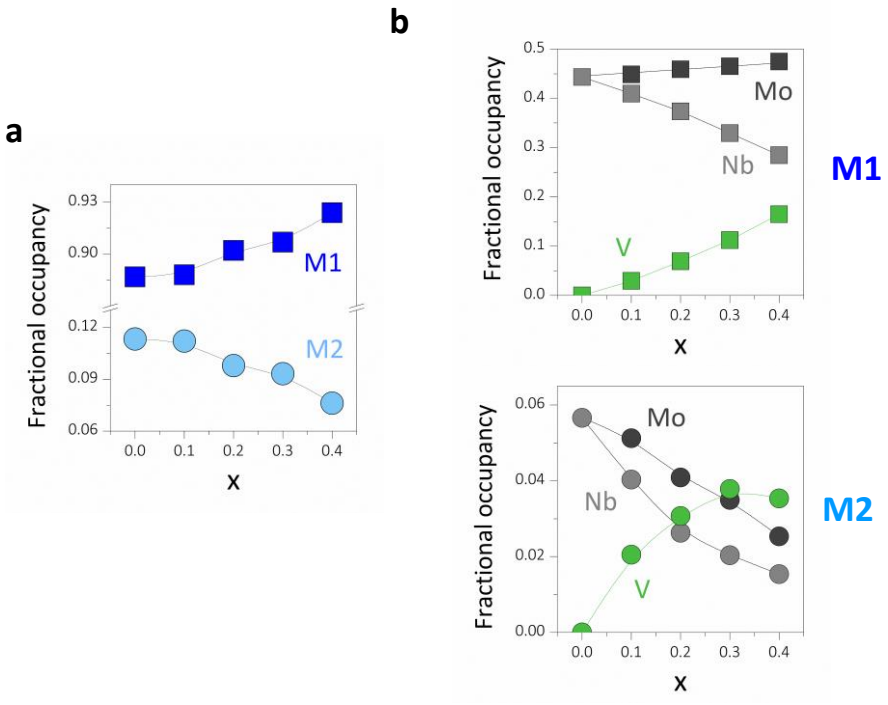

Supporting Figure S18. Variation of the total (a) and individual (b) metal fractional occupancies in the $Ba_3Nb_{1-x}V_xMoO_{8.5}$ (x = 0.0, 0.1, 0.2, 0.3, 0.4) series.

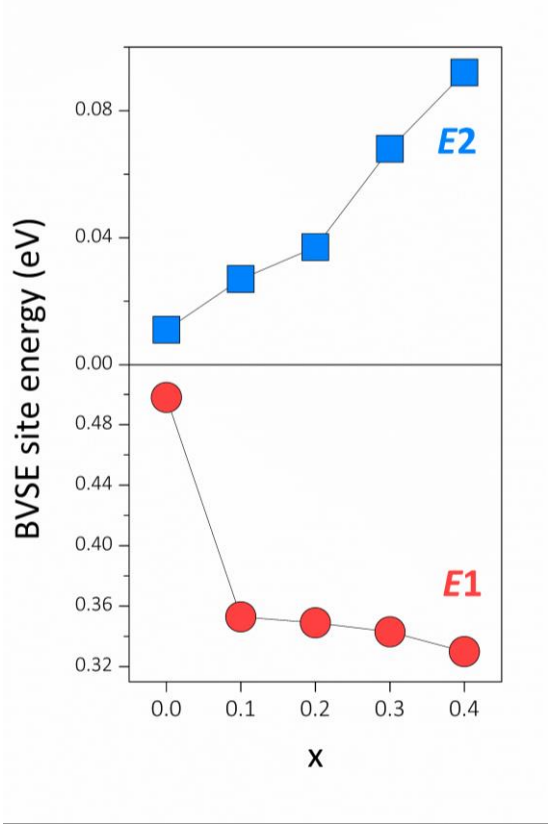

Supporting Figure S19. Variation of *E*1 and *E*2 with V-doping in the $Ba_3Nb_{1-x}V_xMoO_{8.5}$ (*x* = 0.0, 0.1, 0.2, 0.3, 0.4) series.

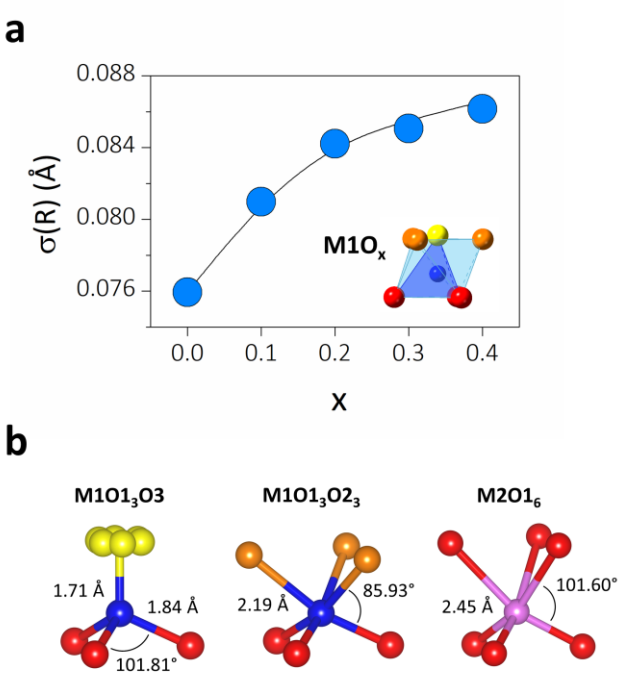

Supporting Figure S20. (a) average distortion of the $M1O_x$ polyhedral units as calculated by the PIEFACE software plotted against the amount of V doping, *x*. (b) Average coordination units in $Ba_3NbMoO_{8.5}$ with selected bond lengths and angles highlighting the polyhedral distortion.

References

[1] Boukamp, B. A. A linear Kronig-Kramers transform test for immittance data validation. *Journal of The Electrochemical Society* **1995**, *142*, 1885-1894.

[2] Boukamp, B. A. Electrochemical impedance spectroscopy in solid state ionics: recent advances. *Solid State Ionics* **2004**, *169*, 65-73.

[3] Fop, S.; Skakle, J. M. S.; McLaughlin, A. C.; Connor, P. A.; Irvine, J. T. S.; Smith, R. I.; Wildman, E. J. Oxide ion conductivity in the hexagonal perovskite derivative $Ba_3MoNbO_{8.5}$. *J. Am. Chem. Soc.* **2016***, 138*, 16764-16769.

[4] Irvine, J. T. S.; Sinclair, D. C.; West, A. R. Electroceramics: characterization by impedance spectroscopy. *Adv Mater* **1990***, 2*, 132-138.

[5] Li, M.; Pietrowski, M. J.; De Souza, R. A.; Zhang, H.; Reaney, I. M.; Cook, S. N.; Kilner, J. A.; Sinclair, D. C. A family of oxide ion conductors based on the ferroelectric perovskite $Na_{0.5}Bi_{0.5}TiO_3$. *Nature Materials* **2013***, 13*, 31-35.

[6] Verbraeken, M. C.; Cheung, C.; Suard, E; Irvine, J. T. S. High H^- ionic conductivity in barium hydride. *Nature Materials* **2014**, 14, 95-100.